communications materials

Article

https://doi.org/10.1038/s43246-024-00724-9

Predictive design of tactile friction for micro/nanostructured haptic surfaces

Check for updates

Yuan Ma [1,2,3,5], Xinyi Li [1,5], Xuezhi Ma [1,4], Changhyun Choi [1], Luke Kruse [1], Shoufeng Lan [1] & M. Cynthia Hipwell [1] ✉

Design of micro/nanotextured consumer product surfaces presents the opportunity to enrich tactile experiences and enhance the capabilities of haptic devices, enabling rich human-object interactions through the passive or active control of finger friction. The absence of a comprehensive model that can holistically represent the underlying physics at finger-material interface, however, inhibits reliable prediction of finger friction. Here, we develop a model for micro/nanostructured touch interfaces, accounting for contact mechanics, capillaries, electrostatic fields, and their mutual interactions. We experimentally validate this model and apply it to predicting the friction and adhesion of microparticle-coated plastic films for food packaging, and designing surface structures for electroadhesive surfaces to achieve both stronger effects and lower variability — essential features for high-volume consumer electronics. Our model has wide applicability in predictive design of micro/nanostructured surfaces with diverse haptic functionalities.

The sense of touch, essential and fundamental to human perception, enables us to explore, interact with, and navigate the physical world through mechanoreceptors distributed within the skin (Fig. 1A). Beyond its inherent role in perceiving textures, pressures, and temperatures, tactile perception also profoundly influences our affective and aesthetic preference for objects[1,2]. From consumer electronics to cosmetics to food packaging, surface modifications through texturing and coating have been employed to reduce adhesion and friction, thus providing a "pleasant" or "high-quality" tactile feeling[3,4]. The conventional trial-and-error approach, which involves experimentally testing different combinations of surface properties including surface textures, Young's moduli, and surface energies, is inefficient and inadequate to find the optimal design. Moreover, at the finger-material interface, complex multiphysics interactions arising from the contact mechanics across scales[5,6], capillaries resulting from adsorbed water and human sweat[7–9], as well as the presence of sebum and lipids, further complicate the problem. These interactions pose significant challenges to accurately and realistically predicting finger friction on micro/nanotextured surfaces — crucial for predictive design of surfaces with desirable tactile feeling.

For active simulation and modulation of sense of touch with haptic technologies, a diverse spectrum of novel materials and devices has been created for both sensing and rendering, allowing users to interact with both the real and virtual world via interactive screens and wearable devices[8,10–15]. As one of the most promising device platforms, electroadhesion-based surface haptic technologies have been successfully demonstrated. By modulating the friction force through an electrostatic field between the human finger and the screen surface, electroadhesion can create virtual tactile sensations on touchscreens[16,17]. Despite its initial success in technology demonstration, however, challenges remain for surface haptic technology to achieve effective and realistic tactile feedback due to the complexity and variability of finger-screen contact interfaces. For high-volume consumer electronics, it's paramount to simultaneously attain a strong electroadhesion effect and low variability against environmental and user conditions. Previous studies have demonstrated that the variability of the electroadhesion effect results from the interactions between capillaries and electrostatic field[8]. These interactions are very sensitive to the topography of the screen surface[7], indicating the possibility of optimizing the electroadhesion performance of surfaces through intentionally designing nano and microscale surface structures. This design optimization process, however, has traditionally relied on the time-consuming and costly trial-and-error process. Current devices are optimized by fabricating and testing numerous prototypes with varying glass textures and coatings. To achieve successful forward prediction and design of micro/nanostructured surfaces for desirable frictional behavior and device performance, a model that accurately captures the governing multiphysics across scales is of paramount importance. In addition, the texture often needs to meet optical requirements, being of a

[1]Department of Mechanical Engineering, Texas A&M University, College Station, TX, 77840, USA. [2]Present address: Department of Mechanical Engineering, The Hong Kong Polytechnic University, Kowloon, Hong Kong. [3]Present address: Research Institute for Intelligent Wearable Systems, The Hong Kong Polytechnic University, Kowloon, Hong Kong. [4]Present address: Institute of Materials Research and Engineering, Agency for Science, Technology and Research, 2 Fusionopolis Way, Innovis, #08-03, Singapore, 138634, Singapore. [5]These authors contributed equally: Yuan Ma, Xinyi Li. ✉e-mail: cynthia.hipwell@tamu.edu

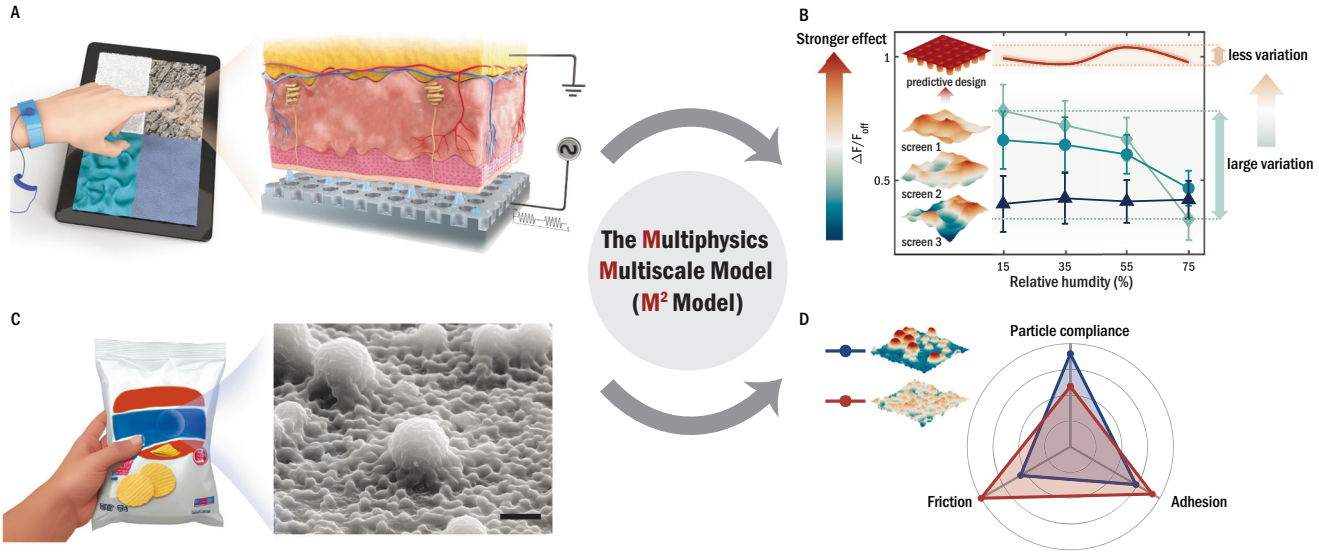

Fig. 1 | The Multiphysics Multiscale Model (M^2 Model) for improved prediction of tactile friction of micro/nanostructured haptic surfaces. A Schematic illustration of a finger in contact with an electroadhesive touchscreen that can render virtual textures. The zoomed-in view shows the skin with its multilayer structure (stratum corneum, visible epidermis, dermis, and subcutaneous tissue) and sweat glands and the eletroadhesion substrate with oxide layer. At the interface, capillary bridges are formed with sweat, lipids, and adsorbed water from the environment. **B** Measured electroadhesion effect ($\Delta F/F_{off} = (F_{on} - F_{off})/F_{off}$) for three electroadhesive touchscreens with stochastic nanotextures. The red line schematically shows the desirable optimized electroadhesion performance with strong effect and reduced variability that can be achieved with predictively designed micro and nanostructures. Insets are surface topographies characterized with an atomic force microscope (Jupiter XR AFM, Oxford Instruments). **C** Schematic illustration of a hand holding a textured plastic food package. The zoomed-in view shows microparticles coated on the plastic film imaged with a scanning electron microscope (LYRA-3 Model GMH FIB-SEM, TESCAN). The scale bar is 3 μm. **D** Radar plot comparing two plastic films coated with large microparticles (blue) and small microparticles (red): friction is represented by the modeled real contact area, adhesion is represented by the modeled capillary force, particle compliance is defined as the ratio of indentation depth and normal load, which is the inverse of stiffness (Supplementary Table 6). The legend shows the surface topographies of the two samples characterized with an atomic force microscope (Jupiter XR AFM, Oxford Instruments).

nanoscale size below the wavelength of light, designed to be transparent and sometimes with added features, such as anti-glare. To meet two critical requirements simultaneously, further drives the need for models which enable co-design.

Pioneering works by Adams et al.[18–20] adopted Bowden and Tabor's expression of adhesive friction[21] to model fingerpad friction, where friction is proportional to the real contact area and the interfacial shear strength, and utilized Hertzian contact model to estimate the gross contact area by approximating the fingerpad as the cap of an elastic sphere. This approach laid the groundwork for recent models of finger friction. In the context of electroadhesion, Shultz et al.[16] first developed a lumped impedance model for the electroadhesive force between skin and electroadhesion surface haptics, highlighting the importance of the accurate description of the textured contact gap. This foundational work paved the way for subsequent studies that have focused on understanding and modeling finger friction on textured surfaces, which is essential for the design and optimization of haptic devices. Among these efforts, Persson's contact theory[22–24] stands out for its ability to predict the real contact area considering the surface texture at different scales based on the surface roughness power spectrum. Its application has been successfully extended to electroadhesion touchscreens[22,23,25]. In light of this method, Forsbach et al.[26] further adopted a two-scale approach using a microscale bearing area model (BAM) to calculate air contact gap size with surface roughness power spectrum and incorporate this gap size into a macroscale finite element model (FEM) finger contact model. These power spectrum based contact models, developed for randomly rough surfaces, cannot accurately describe non self-similar surfaces, which are often the case for intentionally designed surface textures. Moreover, electrowetting, as the result of the interaction between capillary and electric field, was found to be an important effect to consider for electroadhesive devices[27,28], but none of these aforementioned models directly coupled capillary and electric field. Recently, a model at the single-asperity level was developed to consider the coupling effects of multiphysics interactions with specific geometries of individual asperities which are not limited to self-similar surfaces[7]. This model has successfully demonstrated the impact of asperity shapes and surface energy on eletroadhesion effect and explained the counterintuitive results of the friction of two plastic films with different skin conditions[29]. The interactions between neighboring asperities as well as the finger surface topography, however, were missing in the single asperity model. Due to their intrinsic limitations, none of these works can holistically model the friction and adhesion of arbitrarily micro/nanotextured surfaces for prediction and design.

Here, we demonstrate a multiphysics multiscale model (M^2 Model) for micro/nanostructured touch interfaces which can serve as the governing model to predict the friction and inversely design micro/nanostructures for finger-material interfaces as well as the next-generation of haptic devices. This model is experimentally validated, as we show that it can predict the electroadhesion performance of micro/nanostructured haptic interfaces by simultaneously considering contact mechanics, capillaries, electrostatic fields, and their interactions with surface textures across scales (Fig. 1A). Based on this model, we designed a structure for electroadhesion-based surface haptics that can achieve high friction force modulation while maintaining a small variation with changing relative humidity (RH) (Fig. 1B). This model can be more generally applied to a broad variety of surfaces. We utilized this model to predict the friction, adhesion, and compliance of microparticle-coated plastic films (Fig. 1C) and explain counterintuitive results for measured friction with different finger status (Fig. 1D).

Results and discussion

As mentioned in the introduction, electroadhesion-based surface haptic devices vary in their performance with environmental conditions and user sweat[27]. To demonstrate this effect, the finger friction force of multiple volunteers on three electroadhesive touchscreens used in commercial devices was measured at controlled RH. The three surfaces have similar

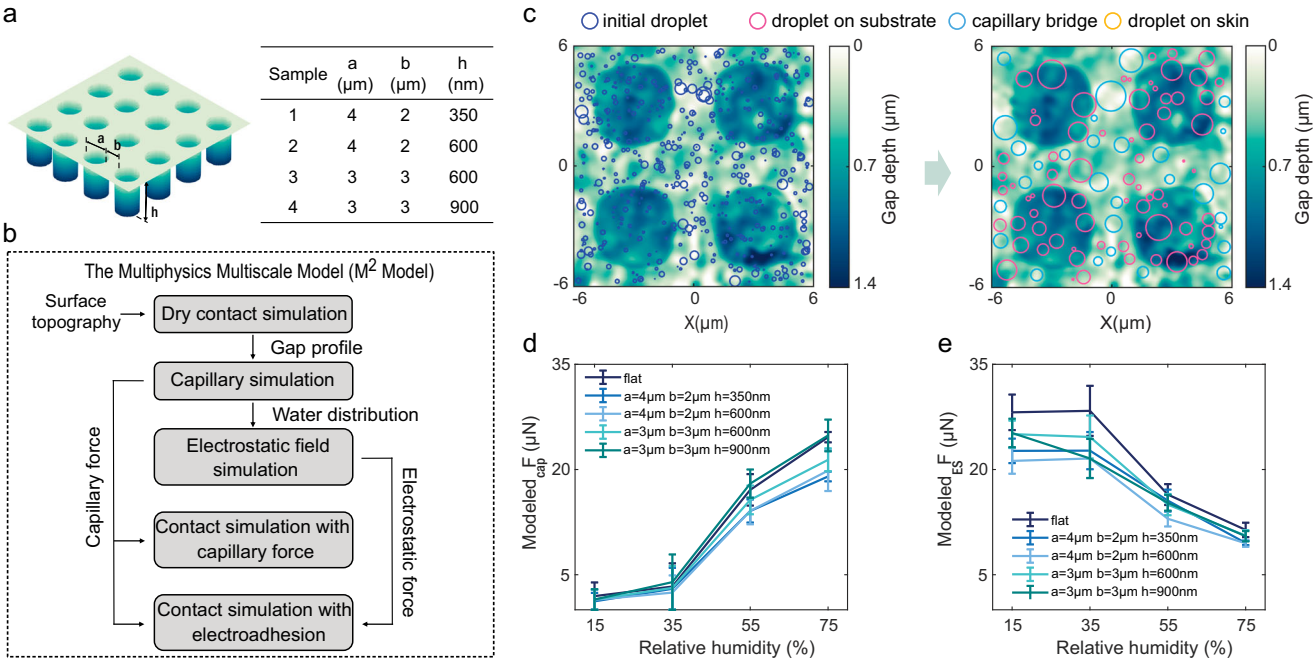

Fig. 2 | The multiphysics multiscale model (M^2 Model) for micro/nanostructured haptic interfaces. a Electroadhesive surfaces structured with micro/nano scale hole arrays with their nominal parameters. The measured parameters are summarized in Supplementary Table 1. **b** Flow chart of the M^2 model. **c** Capillary simulation at the micro/nanostructured interface: the initial random distribution of 500 tiny water droplets with a total water volume of 5 μm^3 (left) and the final distribution of capillary bridges and water droplets on the substrate and on the skin. Note that in this case, there are no droplets on the skin because it has a higher contact angle than the substrate which is energetically unfavorable. **d** Modeled capillary force for the simulated 12×12 μm^2 area. Each data point is the average of results simulated with the water volumes in Supplementary Table 4 for each relative humidity and the error bar represents the upper and lower limits. **e** Modeled electrostatic force at the effective voltage of a 200 V amplitude AC signal, or the root-mean-squared voltage (V_{rms}) at 141.4 V, and considering the simulated capillary distribution.

stochastic textures resulting from a similar etching procedure, but have different roughness (Supplementary Fig. 1). The percentage of friction force increase by electroadhesion ($(F_{on} - F_{off})/F_{off} = \Delta F/F_{off}$) has been shown to be related to the perceived tactile electroadhesion effect[7,30]. As shown in Fig. 1B, the smoothest surface (screen 1) has the strongest electroadhesion effect, but it also has the largest variation across different RH. Conversely, the roughest surface (screen 3) is much less sensitive to humidity change, but has the weakest electroadhesion effect. None of these situations are desirable for product performance and this example of supplied screen samples demonstrates the limitations of trial-and-error experimentation. It is desirable then, to be able to understand how to decouple the electroadhesion effect from its sensitivity to external environments and purposely design a screen with high electroadhesion effect and low variability.

To achieve successful decoupling and parameter control, we developed the M^2 model, which accounts for important multiphysics in the micro/nanostructured haptic interfaces: contact mechanics, electrostatics, capillaries, finger tissue deformation, multiscale texture, and changing finger mechanical properties (modulus) in our model. The following sections detail each of those calculations. The model focuses on modeling the adhesive friction, lubrication was not considered: Peng et al.[31] showed that to have finger friction in the elastohydrodynamic lubrication (EHL) regime, the fluid film thickness needs to be at least several microns, which requires the presence of extra lubricant at the interface. The forces addressed by the M^2 model include contact force, electrostatic force, and capillary force (surface tension and capillary pressure), which have been demonstrated to be the most essential and dominant forces to include[7,22,23,27]. The van der Waals force was calculated based on Hamaker's theory[32] and was considered too small to significantly impact the interactions in our system and can therefore be neglected (see Supplementary Text 1). The retention forces from contact angle hysteresis (CAH) were observed to be significantly smaller than the increased friction by capillary adhesion and were thus neglected, except for their contribution to the electroadhesion effect in hydrophobic samples (see Supplementary Text 5). The interfacial shear strength (τ) was assumed to be constant at 9 MPa[22]. These assumptions allowed for a more tractable and focused analysis of the key mechanisms influencing finger friction on electroadhesive touchscreens.

Contact mechanics analysis considering skin modulus change with moisture

The stratum corneum (SC) is the outermost layer of skin that directly interacts with the external environment. It is composed of multiple layers of disk-like corneocytes with diameters of 30~40 μm and thickness of 0.5~1 μm[33,34]. In our M^2 model, the first layer of the SC was modeled as a 1 μm thin plate of stiffer material with real finger surface micro/nanoscale textures[5]. The rest of the layers of the SC were modeled as a thicker and softer bulk material (Supplementary Fig. 2). The elastic moduli of the two layers were set to decrease linearly with increasing RH[35] as measured in the literature[36,37] and summarized in Supplementary Table 2. The contact mechanics analysis of the M^2 model was first performed with preload, which provides the topological foundation for the capillary simulation and electrostatic analysis. (See Supplementary Text Section 1 for further details of the contact analysis).

Capillary simulation for micro/nanostructured interfaces

A key aspect of the micro/nanostructured haptic interface is capillaries from finger sweat, lipids, and condensed water[7,8]. Capillaries contribute to finger friction force by increased normal contact area and contact angle hysteresis (CAH). In the M^2 model, both effects are considered. The increase of normal contact area induced by capillary force was calculated using the gap profile between the skin and the substrate after the contact mechanics analysis with preload. A given total volume of water was randomly distributed in the gap geometry in the form of many tiny droplets (100 droplets per μm^3) with random initial volumes (Fig. 2c, Supplementary Fig. 6). The number of initial droplets was chosen based on a previous study to ensure the good model convergence[27].

The droplets were then allowed to move freely with a small step size and would coalesce with each other if they overlaped. Each droplet could be in one of the three states: droplet attached to the skin, droplet attached to the substrate, or forming a capillary bridge between the skin and the substrate. The status and the position of each droplet were determined by minimizing its total surface energy with given contact angles on both surfaces given by:

$$\begin{cases} Minimize\ F(r,\boldsymbol{x}) = A_{lv}(r,\boldsymbol{x},h_1(\boldsymbol{x}),h_2(\boldsymbol{x})) - A_{ls1}(r,\boldsymbol{x},h_1(\boldsymbol{x}))\cos\theta_1 - A_{ls2}(r,\boldsymbol{x},h_2(\boldsymbol{x}))\cos\theta_2 \\ Subject\ to\ v(r,\boldsymbol{x},h_1(\boldsymbol{x}),h_2(\boldsymbol{x})) = v_0 \\ max(\boldsymbol{x}_0 - \Delta\boldsymbol{x}_{max}, \boldsymbol{x}_{min} + r) < \boldsymbol{x} < min(\boldsymbol{x}_0 + \Delta\boldsymbol{x}_{max}, \boldsymbol{x}_{min} - r) \end{cases} \quad (1)$$

where r is the droplet radius, $\mathbf{x} = (x, y)$ is the center location of the droplet, $\mathbf{x_0}$ denotes the original location, $h_1(\mathbf{x})$ and $h_2(\mathbf{x})$ are the heightmaps of two surfaces, A_{lv}, A_{ls1}, A_{ls2} are the surface areas of the liquid-vapor interface and the liquid-solid interfaces of the two solids respectively, v is the volume of the droplet, v_0 is its original volume, $\mathbf{\Delta x_{max}}$ is the maximum step size, $\mathbf{x_{min}}$ and $\mathbf{x_{max}}$ are lower and upper bounds of the simulated area, θ_1 and θ_2 are the water contact angles on the two surfaces. The skin contact angle was set to 80° according to literature values[7,22] and the substrate contact angle was set to 50° according to contact angle measurement results (Supplementary Fig. 5a).

This procedure was iterated until all the droplet locations converged locally (Supplementary Scheme 1). With the converged droplet distribution (Fig. 2c, Supplementary Fig. 6), the capillary force of each capillary bridge was calculated using Kelvin's equation for meniscus radius[38] and the total capillary force F_{cap} was obtained by summing up the forces from all of the capillary bridges:

$$F_{cap} = \sum \gamma\left(\frac{1}{R_1} + \frac{1}{R_2}\right) \quad (2)$$

where γ is the surface tension of the liquid, and R_1 and R_2 are the principal radii of each capillary bridge.

The water volumes were estimated based on human sweat rates and water evaporation rates at different RH (see Supplementary Text Section 3 for details). Each water volume was simulated 6 times independently and the averaged capillary forces are summarized in Supplementary Table 4 and shown in Fig. 2d. The capillary forces of the capillary bridges were applied as nodal forces at their location in the contact mechanics model along with the preload to simulate the real contact area.

In the meantime, the friction force from CAH was also calculated (see Supplementary Text Section 5). The line retention force from CAH was observed to be more than one order of magnitude smaller than the increased friction by capillary adhesion for two asperities in contact[7]. Since most of the asperities at the interface are not in real contact with each other, numerous capillary bridges formed between non-contacting asperities also contribute to the overall friction[39]. The retention forces from all of the capillary bridges were calculated and found to contribute only ~ 5% to the total "off" friction with simulated water volume up to 10 μm^3 for the hydrophilic samples (Supplementary Fig. 5b, Table 4) and were, therefore, neglected. The CAH contribution to the electroadhesion effect for hydrophobic samples, however, was considered.

Coupling capillaries and the electrostatic field

Two competing effects exist for capillaries in an electric field: 1. the electrowetting-on-dielectric (EWOD) effect[40], where the applied electric field decreases the water contact angle on the substrate (usually starting with a hydrophobic contact angle) and thus the capillary force increases; 2. The electrostatic effect, where the existence of a capillary bridge at the contact gap greatly reduces the overall strength of the electric field, and thereby decreases the electrostatic force. These effects were first studied at the single asperity level in published work[7] and the conclusions are used to inform the model in this work. To quantitatively study these competing mechanisms in the M^2 model, the electrostatic field was first simulated with the skin geometry and substrate deformed with preload. Based on the droplet distribution achieved in the capillary simulation step (Fig. 2c), the electrostatic field was updated: if a node was covered by a capillary bridge or a water droplet, its nodal electrostatic force was removed. Calculated based on the single asperity model results, a correction factor was applied to the electrostatic forces on the rest of nodes (see Supplementary Text Section 4, Supplementary Fig. 4). Finally, the corrected electrostatic forces (Fig. 2e, Supplementary Table 4), capillary forces (Fig. 2d, Supplementary Table 4) and preload were applied simultaneously to the contact mechanics model to simulate the total real contact area with electroadhesion effect with different humidity conditions (Supplementary Table 4).

Predicting finger friction and electroadhesion effect

To model the total friction force, a macroscale whole finger model (Supplementary Fig. 3, Supplementary Table 3) was built to simulate the apparent contact area (A_{app}) and preload for the microscale model (Supplementary Text 2, Supplementary Table 2). We have employed the Bowden-Tabor theory to model the friction force between fingers and micro/nanotextured surface[21,41], as it provides a more fundamental description of the tribological behavior of adhesive friction at the asperity level, allowing us to incorporate the asperity-level considerations of surface texture, capillary force, electroadhesive force, etc.

$$F = \tau A_{real} \quad (3)$$

$$A_{real} = A_{app}\frac{A_{real\ micro}}{A_{micro}} \quad (4)$$

where τ is the interfacial shear strength, assumed to be constant at 9 MPa[22]. A_{real} is the total real contact area for the whole finger, $A_{real\ micro}$ is the real area in contact simulated by the microscale model, and A_{micro} is the simulated area of the microscale model, which is $12 \times 12\ \mu m^2$ in this case.

It is well-documented in the literature that asperity based contact models with a statistical description of asperity distribution, such as the Greenwood–Williamson (GW) model[42] and the models developed based on the GW model[43–45], can be used to predict macroscopic contact behaviors. Instead of relying on statistical models, the M^2 model utilizes a multiasperity model to describe the actual asperity distribution, which in most cases are non-Gaussian. In addition, the multiasperity model also captures the multiphysics at the microscale, and this was informed by the single asperity model where the fundamental microscopic physics of the capillary-electric field interactions were modeled[7]. These interactions are crucial for understanding the frictional behavior but are challenging to model directly across an entire macroscopic surface due to the computational resources required at micro/nanoscale resolution.

We validated the individual model components via individual first principles calculations and in the single asperity model of our previous work[7], and then validated the full multiphysics model via comparison to measured experiments over multiple conditions and multiple materials. The relevant metrics included: 1) can the model correctly predict the trends and orders (since dry contact models do not predict the experimental results) and 2) magnitude of friction. For practical design use, model-measure closure metric 1) is essential within the relevant range and 2) we want to get as close as possible. In our validation, the model was able to replicate the impact of RH and surface structures from the experimental results, which showed that both F_{off} and F_{on} increased nearly two-fold for all the samples at RH ranging from 15% to 75% (Fig. 3a, d). This increase in force can be attributed to the decrease of skin modulus with absorbed moisture, resulting in a remarkable ~58.5% increase in the apparent contact area and a ~45.5% increase in the microscopic real contact area. In addition, the model predicted that capillary force contributes up to about 22.3~24.1% additional increase of the microscopic contact area at 75% RH, with water volumes ranging from 5 to 10 μm^3. Samples with larger holes were shown to have lower friction forces due to smaller capillary forces (Figs. 2d and 3d): Samples with 4 μm holes have lower capillary forces than Samples with 3 μm

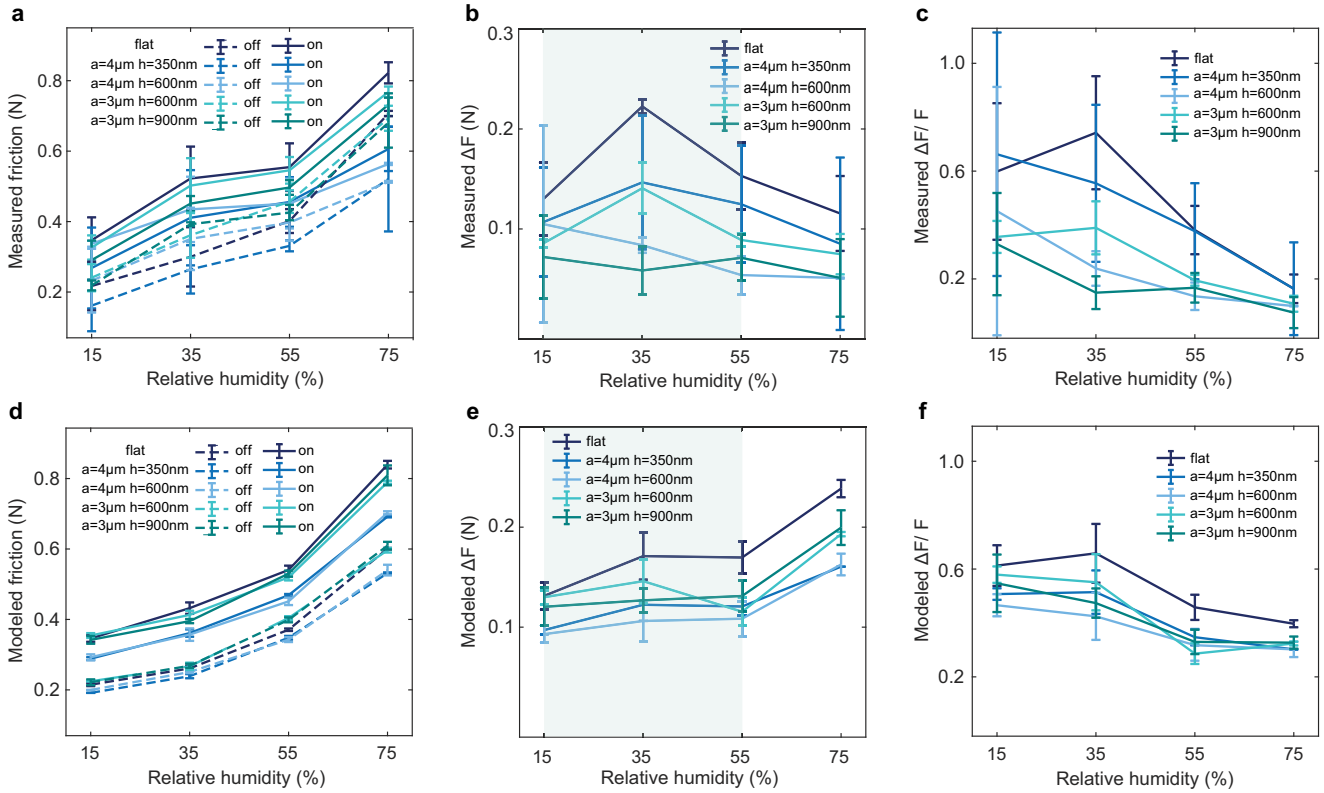

Fig. 3 | Model validation with experimental measurement. a Measured friction force with electroadhesion turned on and off with a 5 kHz 200 V amplitude AC signal. Each data point is averaged from three repeated measurements and the error bars represent the standard deviation. (See Methods) **b** Measured friction force increase ($\Delta F = F_{on} - F_{off}$) by electroadhesion. **c** Measured electroadhesion effect ($\Delta F/F_{off}$). **d** Modeled friction force with each data point is the average of results simulated with the water volumes in Supplementary Table 4 for each relative humidity and the error bar represents the upper and lower limits. The "on" frictions were modeled at the effective voltage of the 200 V amplitude AC signal, or the root-mean-squared voltage (V_{rms}) at 141.4 V. **e** Modeled friction force increase ($\Delta F = F_{on} - F_{off}$) by electroadhesion. **f** Modeled electroadhesion effect ($\Delta F/F_{off}$).

holes at 55% and 75% RHs with 95–99.9% of confidence levels based on t-tests performed on the 6 independent simulation results. This can be explained by the tendency of liquids to minimize their surface energy. In such cases, capillary bridges would be more stretched and less likely to form inside the hole (Supplementary Fig. 7). For samples with different hole depths, no statistically significant difference was found between 350 nm, 600 nm or 900 nm, which indicates that capillaries are hard to form inside the hole even with the shallowest hole depth of 350 nm.

The model also showed good agreement with experiments in terms of $\Delta F/F_{off}$, which has been shown to be proportional to the perceived electroadhesion effect[7,30]: samples with smaller ($a = 3$ μm $h = 600$ nm v.s. $a = 4$ μm $h = 600$ nm) or shallower holes ($a = 4$ μm $h = 350$ nm v.s. $a = 4$ μm $h = 600$ nm, and, $a = 3$ μm $h = 600$ nm v.s. $a = 3$ μm $h = 900$ nm) have higher electrostatic forces, thus stronger electroadhesion effect, however, they also have larger variation across humidities; samples with larger or deeper holes have weaker but more consistent effect with smaller electrostatic forces and capillary forces (Fig. 3c, f). Overall, these findings demonstrate the efficacy of the model in predicting the relative behavior of skin friction under varying conditions of moisture and surface texture geometry.

Instead of relying on statistical models or surface roughness power spectrum to represent surface textures like GW based models and Persson's model, the M^2 model directly incorporates scanned surface topography from characterization tools such as AFM. This allows it to more accurately simulate the effects of distinct, intentionally designed textures without approximations. Additionally, the model's sensitivity in predicting increases in microscopic contact area due to capillary forces, as well as its differentiation of frictional responses based on hole size and depth, underscores its usefulness in simulating practical design conditions. The experimental model validation was conducted through a comprehensive series of tests involving multiple samples with diverse surface textures and systematically varied RH, offering a robust dataset for comparison with model predictions. This validation confirms that the M^2 model is not only theoretically sound in its inclusion of important phenomena, but also practically useful in predicting skin friction behavior under varying moisture and surface texture conditions.

Parametric study of the model can provide further insights into the physics of the moisture mediated friction force for the electroadhesion effect. While capillary force is a secondary effect in increasing the base friction force with RH, it plays a critical role in the electroadhesion effect. As shown in Fig. 3b, e, both the model and experimental results predicted that ΔF first increased between 15% to 35% RH and then decreased between 35% to 75% RH for samples with shallower or smaller holes (flat sample, $a = 4$ μm $h = 350$ nm and $a = 3$ μm $h = 600$ nm). For samples with deeper or larger holes ($a = 4$ μm $h = 600$ nm and $a = 3$ μm $h = 900$ nm), however, ΔF slightly decreased or remained constant with increasing RH. These trends of ΔF are closely related to the presence of capillaries inside the electrostatic field, as softer tissue alone leads to larger contact area increase, which always results in higher ΔF at higher RH. With hydrophilic samples, the electrostatic field was reduced with more capillary bridges formed at higher RH without significant electrowetting effect (Fig. 2e). The model captured these competing mechanisms well, demonstrating that for samples with shallower and smaller holes (i.e., flat sample, $a = 4$ μm $h = 350$ nm, and $a = 3$ μm $h = 600$ nm), ΔF increased initially from 15% to 35% RH due to the change in skin modulus followed by the decreasing trend at higher RH, indicating that the electrostatic field reduction by capillaries took over. On the other hand, for samples with deeper and larger holes (i.e., $a = 3$ μm $h = 900$ nm and $a = 4$ μm $h = 600$ nm), ΔF remained more consistent. We also noticed a

discrepancy between the modeled ΔF and measured ΔF at the highest humidity levels (Fig. 3b, e), which can be explained by several possible factors. Firstly, in this work, the interfacial shear strength τ has been assumed to be constant. In reality, however, the interfacial shear strength may also decrease slightly at higher RH[46]. The constant shear strength assumption was made partially due to the lack of quantitative correlation between interfacial shear strength changes at high RH. Secondly, if at higher RH, small gaps at nano/microscale are flooded with extra amount of water, micro-elastohydrodynamic lubrication (micro-EHL) may occur[31,47]. Such factors are not captured in this model. Furthermore, large water droplets spanning across multiple holes may form at higher RH. In this case, the pinning effect at the edges of the holes will also contribute to the friction force[48,49]. Nonetheless, these effects are only significant at very high RH levels, and the validity of the M^2 model remains acceptable within a reasonable RH design range.

Predicting friction and adhesion for microparticle-coated plastic films

Li et al.[29] showed that the friction between the finger and plastic packaging could not be simply explained by the dry finger friction models, and the skin surface energy change due to sebum and capillary formed by sweat need to be considered. To verify the utility of the M^2 model in predicting friction, adhesion, and compliance under different finger conditions (isopropyl alcohol (IPA) cleaned finger and finger in natural state with sweat, sebum, and lipids) for consumer product design, two high-density polyethylene (HDPE) films coated with microparticles of different radii (~3 μm and 1.5 μm, respectively) and Young's moduli (~2.6 MPa and 7 MPa, respectively) for food packaging were measured and modeled here (see surface topographies in Supplementary Fig. 9). Prior psychophysical studies have concluded that lower friction and adhesion generally lead to more pleasant tactile feeling[3,4], so this is often the target of tactile consumer product surface and packaging design, adding texture to reduce contact area and friction. This is the case for these packages, with it being predicted that additional texture created by the small particles would result in lower friction and therefore a more pleasant design. The presence of sebum and lipids on the natural fingertip, however, also affects the finger friction and the tactile perception in different ways that must be considered: 1. lipids reduce the water contact angle on skin[50,51], which leads to higher capillary force; 2. the interfacial shear strength is reduced with thicker lipid films[19,52].

For the IPA-cleaned fingers, where sweat and sebum are removed, the M^2 model predicts the sample coated with larger and softer particles has a relatively larger dry contact area, and thus a higher friction force, as would be expected (Fig. 4a). For fingers in natural state (hydrophilic), however, the sample coated with smaller particles is calculated to have higher capillary force with more capillary bridges formed (Supplementary Table 6) which leads to larger contact area and higher friction (Fig. 4a). Capillary bridge distributions on the two samples clearly explain this trend: with the same amount of water, fewer and larger capillary bridges are formed on the large particle-coated sample while more and smaller capillary bridges are formed on the smaller particle-coated sample (Supplementary Fig. 10). Qualitative discussion of capillary force enhancement by capillary bridge splitting can also be found in the literature[53,54]. Note that this result is the opposite of what might be expected from intuition, which would predict that the more textured small particle-coated film would have lower friction.

The model prediction was validated with friction force measurements (see Methods). As predicted by the model, with IPA-cleaned fingers, the small particle-coated plastic film has lower friction, whereas with the finger in natural state, it has higher friction force (Fig. 4b). We also noticed that the measured friction of the large particle-coated sample is higher with the clean fingers than with the natural fingers, but the model suggests that both samples have larger contact area with the natural finger than with the clean finger. This can be possibly explained by the interfacial shear strength reduction with thicker lipids on natural skin[19,52]. Even though the contact area is slightly increased with capillary force, it's possible that the interfacial strength reduction is more dominant and results in lower friction force with the natural finger for the large particle coated sample. For the small particle-coated sample, however, the capillary force increase is significant, and possibly has a more dominant effect over the interfacial strength reduction.

Designing electroadhesive micro/nanostructured haptic interfaces

With the M^2 model, it is possible to achieve different design goals for micro/nanostructured haptic interfaces. As an example, we target here the two most important goals for electroadhesive surface haptic design: 1. strong electroadhesion effect and 2. low variability of the electroadhesion effect under environments with different RH. The first requirement enables lower driving voltage, whereas the second requirement ensures robust surface haptic performance in different markets. Through parametric study of the M^2 model, we found that surface textures with higher aspect ratio tend to mitigate variability caused by capillaries, and that the electroadhesion effect could be enhanced by increasing the initial contact angle of the surface[7,8].

Therefore, an electroadhesive surface structured with 3 μm diameter and 350 nm deep holes (sample 5) and a flat surface were modeled with the original contact angle of 50° and a contact angle of 110° for an assumed hydrophobic coating[7] (Supplementary text Section 6, Supplementary Table 5). The M^2 model predicted that the $\Delta F/F_{off}$ of the hydrophobic surfaces can be enhanced by ~130% in the humid environment compared to the hydrophilic surfaces (Fig. 4e). Moreover, the variation of $\Delta F/F_{off}$ can be further reduced from 27.3% (the flat surface) to 6.7% (the structured surface) (Fig. 4e). Based on these findings, the structured sample was chosen as a direction for optimization and fabricated. This sample and the flat sample were then coated with a hydrophobic coating (Liquid Diamond Shield). The friction forces of the two samples before and after applying the hydrophobic coating were measured (Fig. 4f). The effect of surface energy on friction force can be demonstrated by both modeled and measured friction: lower surface energy (i.e., higher contact angle) leads to lower friction (flat v.s. hydrophobic flat, textured v.s. hydrophobic textured). With electrowetting effect where the contact angle is reduced by electric field, hydrophobic surfaces have stronger $\Delta F/F_{off}$ than the original hydrophilic surface at all humidity levels, as predicted (Fig. 4g, Supplementary Fig. 8). In addition, the textured hydrophobic surface also demonstrated less variations in $\Delta F/F_{off}$ across different humidities. It is important to note, however, that for the hydrophobic samples, the measured $\Delta F/F_{off}$ were much higher than the predicted values with a maximum ~120% of difference at 35% RH and a minimum ~28% of difference at 15% for the flat surface. It is possible that capillary-induced electrostatic field reduction is less on hydrophobic surfaces since droplets are less spread out with larger contact angles. Assuming no reduction in the electrostatic field due to capillaries, a theoretical maximum $\Delta F/F_{off}$ of ~1.38 was found through simulation, which is close to the measured results. In addition, the discrepancy between the modeled and measured $\Delta F/F_{off}$ can be exaggerated with uncertainties in both ΔF and F_{off}. Nevertheless, the model predicts the important relative design order and provides the correct direction of improvement.

The texture design informed by M^2 model could enhance the robustness of products against environmental and user variability. The M^2 model integrates a comprehensive multiphysics approach that simultaneously considers contact mechanics, capillary forces, and electrostatic fields, providing a more holistic understanding of the interactions at the micro/nano level, which is crucial for accurately predicting and optimizing tactile friction. Additionally, The M^2 model emphasizes the role of environmental factors, such as humidity, in influencing tactile friction, a consideration often overlooked in existing models that tend to assume constant environmental conditions. By incorporating these environmental variables, the M^2 model ensures that the designed haptic devices maintain consistent performance across a range of conditions, which is particularly important for real-world applications where users may encounter varying humidity levels and other environmental changes. Moreover, a multiscale model enables co-design with optical models to design surface textures ensuing both haptics and optical performances.

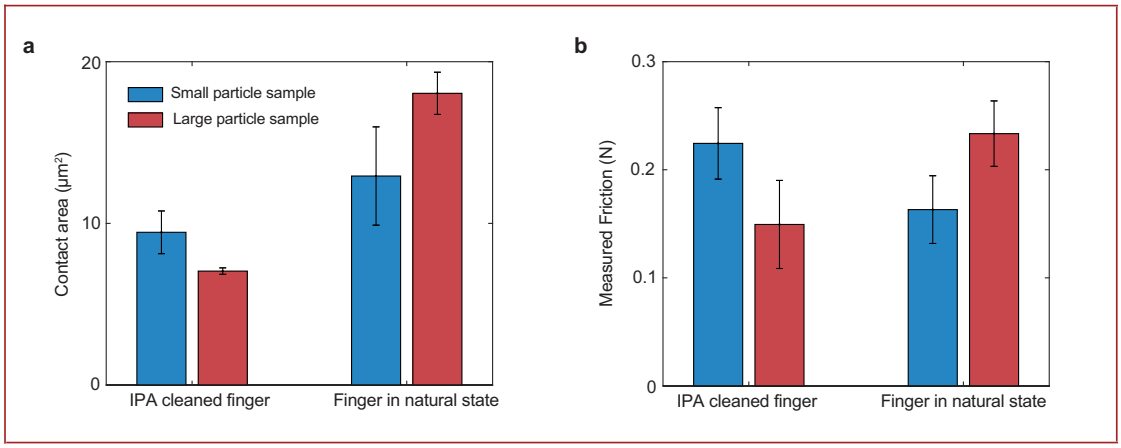

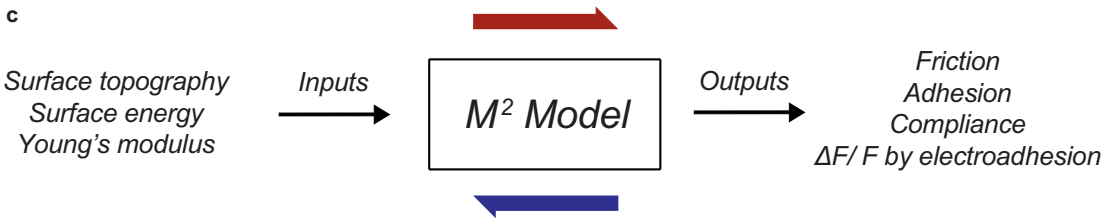

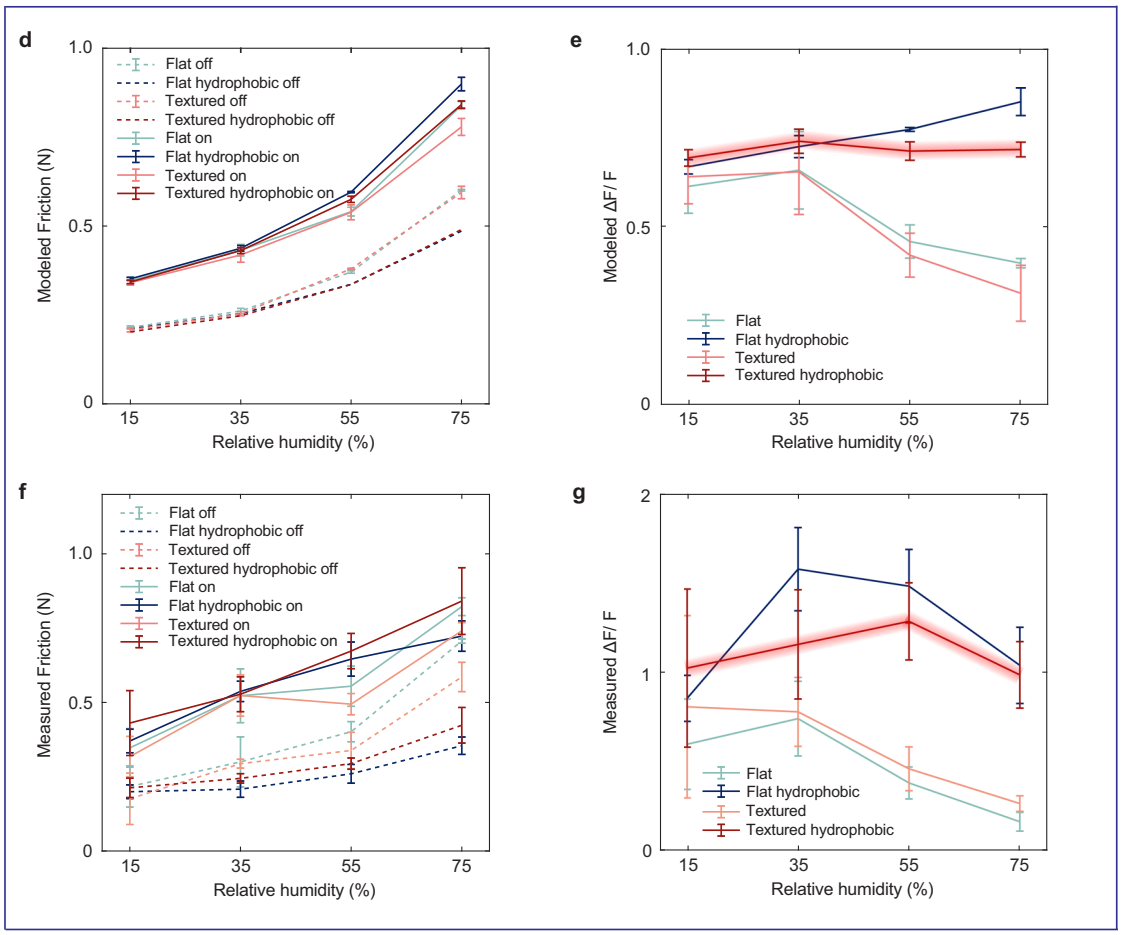

Conclusion

In summary, the M^2 model developed in this work provides a valuable tool for predicting the finger friction on micro/nanotextured surfaces for tactile perception as well as designing surface structures for surface haptics optimization by coupling interfacial multiphysics including contact mechanics, electrostatic field, capillary forces, and electrowetting through iterative numerical simulations. The single asperity model developed in an earlier work was used to accurately capture nanoscale interactions between capillary and electrostatic field and inform the M^2 model. To validate the model and explore the design space, a series of electroadhesive surfaces artificially

Fig. 4 | Model applications for prediction and design. a The modeled real contact of the two plastic films coated with large particles and small particles and with different finger conditions. The error bar represents the standard deviation from independent simulations with three different regions (Supplementary text Section 7, Supplementary Table 6). **b** The measured friction force of the two plastic films at 0.3 N normal load with different finger conditions (see Methods). The error bar represents the standard deviation. **c** Flow chart of the model for prediction (forward) and design (backward) purposes. **d** The modeled friction force. For hydrophilic samples and the "on" friction of hydrophobic samples, each data point is the average of results simulated with the water volumes in Supplementary Table 5 for each relative humidity and the error bar represents the upper and lower limits. For the "off" friction of the hydrophobic samples, capillary force was neglected. The "on" frictions were modeled at the effective voltage of a 200 V amplitude AC signal, or the root-mean-squared voltage (V_{rms}) at 141.4 V. **e** The model predicted ($\Delta F/F_{off}$). **f** Measured friction force at 0.2 N normal load with electroadhesion turned on and off with a 5 kHz 200 V amplitude AC signal. Each data point is averaged from three repeated measurements and the error bar represents the standard deviation. (see Methods) **g** Measured $\Delta F/F_{off}$ (which is correlated to perceived electroadhesion effect).

structured with microhole arrays with different hole diameters and depths were fabricated on silicon substrates. By refining the model parameters including skin modulus, interfacial shear strength, and total water volumes at each relative humidity (RH) level using both experimental and literature data (see Supplementary Text 1 and 2), the model accurately predicted friction forces with and without electroadhesion. Additionally, it successfully forecasted the percentage increase in friction force, which corresponds to the perceived electroadhesion effect under various RH conditions.

Using the M^2 model, the relative order of finger friction and adhesion of two microparticle-coated plastic films for food packaging were successfully predicted considering the complex interactions from sweat and lipids on fingertips. Moreover, a new micro/nanostructured electroadhesive haptic surface with hydrophobicity was designed under the guidance of the model to achieve optimal performance with strong electroadhesion effect and reduced variability. This design was validated with experimental measurements.

The M^2 model provides important theoretical guidance for the forward prediction of finger friction on various surfaces and the inverse design of future haptic structured surfaces with enhanced performance in human-machine interactions. The application of this model can also span from electroadhesion-based surface haptics to a broader range of human-device and human-material touch interactions by elucidating the underlying physics and providing modeling foundations for the further development of haptic surfaces.

Methods

Micro/nanostructured sample fabrication

Fabrication started with a commercial 4-inch heavy N-doped silicon wafer (UniversityWafer, <100> oriented). The periodic hole array with a periodicity of 6 μm and a hole diameter of 4 μm or 3 μm was written on S1818 positive photoresist with a 4000 RPM spin-coating process using a mask-aligner (EVG 610). Then an Inductive Coupled Plasma Reactive Ion Etching (RIE-ICP) cyclic dry etch (Oxford Plasmalab 100) was used to transfer the pattern from the photoresist to the silicon wafer to achieve different hole depths (350 nm, 600 nm, and 900 nm). After removing the S1818 residual photoresist with hot acetone (90 °C) and an oxygen plasma cleaning procedure, a standard wet sacrificed thermal oxidization process was carried out using a commercial thermal oxidation furnace (MiniBrute) at 1100 °C for 40 min. As a result, a 500 nm silicon oxide layer was formed on the silicon structures.

Friction force measurement

The finger friction forces in the paper were measured on a group of 4 volunteers with different genders and ethnicities. Their average age is 25. During these friction tests, the friction force between the volunteers' left index fingers of the volunteers and samples were measured with a custom-built tribometer enclosed in an environmental chamber described in an earlier work[27]. For data consistency and ease of trend comparison, the friction force data in Figs. 2–4 are from the same volunteer. To ensure that this data is representative and not biased, a comparison of different subjects' friction force data on flat samples and on samples with designed microstructures is plotted in Supplementary Fig. 11. This study was approved by the Institutional Review Board of Texas A&M university (IRB ID: IRB2019-0230D) with informed consent obtained from all the participants.

The tribometer consisted of a horizontal linear motor stage (DDS300-E, Thorlabs), a vertical linear stage (VP-5ZA, Newport), two 6-axis force transducers (Nano43, ATI), and a 3D-printed finger holder. The environmental chamber was a glove box with a temperature/humidity controller and sensor (Model 5200-240-230, Model 554, Electro-Tech Systems, Inc.) that could measure humidity levels from 0 to 100% with ±2% accuracy. The tests were conducted at a room temperature of 24 °C and the horizontal stage was set to move at 50 mm s^{-1} with a stroke length of 50 mm. Before each test, both the finger and the samples were cleaned with 70% isopropyl alcohol (IPA) to remove residual sweat and lipids and then acclimatized to the experimental humidity condition for 15 min. Friction forces at different RH were measured in a random order and repeated three times. The normal load was kept constant at 0.2 N using a vertical stage controlled by a PID (proportional–integral–derivative) control algorithm in LabVIEW, which allows the vertical stage to compensate for slight movements of the finger and maintain a constant normal load. To enable electroadhesion, a 5 kHz AC signal with 200 V amplitude turned on and off at 8 Hz was supplied to the silicon substrate. The subject was grounded through an electrostatic discharge band wrist strap. The friction forces with and without electroadhesion effect were extracted from the "on" and "off" periods of the 8 Hz, respectively.

Voltage and frequency are chosen to optimize the electroadhesion effect while minimizing variations in the modulated friction force[17,55]. Higher voltages generally enhance the electroadhesive force by increasing the electric field strength across the interface, thereby improving the attraction between the finger and the surface. However, there is a threshold beyond which further increases in voltage may lead to dielectric breakdown or other adverse effects. Frequency also plays a pivotal role; low-frequency signals tend to produce stronger electroadhesive forces due to longer interaction times between the electric field and the interface, however, it's also less stable with larger variations. Conversely, high-frequency signals can reduce the effectiveness of electroadhesion as the rapid oscillations may not allow sufficient time for the electrostatic forces to stabilize. Shultz et al.[17,55]. have demonstrated that an optimal range of voltage and frequency exists, where the electroadhesion effect is optimized with strong effectiveness and reduced variability without compromising the system's integrity.

For the electroadhesion measurements at different humidity levels, we used 15–75% RH (±2%). This represents a real-world range of variation from coastal and tropical climates which can exceed 80% to desert regions that can go below 20%

For the microparticle-coated plastic films, the friction force was measured at a constant normal load of 0.3 N with the same tribometer without the environmental chamber. Before measuring the friction force of the clean finger, the subject was asked to their wash hands with hand soap, then wipe the left index fingertip with 70% IPA, and wait until the IPA had been fully evaporated. For friction force of the natural finger, there's no intentional cleaning procedure before the measurement. All the measurements were conducted at room temperature (22 °C) and a humidity level of 55% ± 5%, common for an air-conditioned environment.

Prevention for electrical breakdown

The typical electrical field strength that may lead to the breakdown of air is approximately 3 MV m^{-1}, while for silicon dioxide (SiO_2), the dielectric breakdown strength is around 10 MV m^{-1}. In our experiments, we ensure that the electric field strength remains well below these thresholds.

Specifically, we limit the applied voltage to levels that generate electric fields significantly lower than 3 MV m^{-1} in air and 10 MV m^{-1} in SiO_2. Additionally, we use insulating layers to prevent direct contact between conductive surfaces, further reducing the risk of breakdown.

To safeguard against any unforeseen spikes in electric field strength, we incorporate a 1 mA current regulator into our setup. This current regulator acts as a protective measure by limiting the current flow, thereby preventing excessive current that could lead to electrical breakdown. By maintaining a controlled current, the regulator ensures that the electric field strength does not exceed safe limits, even in the presence of high asperities.

Contact angle measurement

The water contact angle on the flat sample was measured by the sessile drop method. 1–2 μL deionized water droplets were dispensed with a syringe on the sample and imaged with a camera (acA1920-150uc, Basler) using a 5X lens. The water contact angles were then extracted and calculated through MATLAB.

Data availability

All data that support the findings of this study are available in the main text, figures, and Supplementary Information. The data that support the findings of this study are available from the corresponding author upon reasonable request.

Code availability

All code that are used in the main text and Supplementary Information are available from the corresponding author upon reasonable request.

Received: 2 June 2024; Accepted: 18 December 2024;
Published online: 02 January 2025

References

1. Spence, C. & Gallace, A. Multisensory design: Reaching out to touch the consumer. *Psychol. Mark.* **28**, 267–308 (2011).
2. Chen, X., Barnes, C., Childs, T., Henson, B. & Shao, F. Materials' tactile testing and characterisation for consumer products' affective packaging design. *Mater. Des.* **30**, 4299–4310 (2009).
3. Klöcker, A., Wiertlewski, M., Théate, V., Hayward, V. & Thonnard, J.-L. Physical factors influencing pleasant touch during tactile exploration. *Plos One* **8**, e79085 (2013).
4. Chen, X., Shao, F., Barnes, C., Childs, T. & Henson, B. Exploring relationships between touch perception and surface physical properties. *Int. J. Des.* **3**, 67–76 (2009).
5. Choi, C., Ma, Y., Li, X., Ma, X. & Hipwell, M. C. Finger pad topography beyond fingerprints: understanding the heterogeneity effect of finger topography for human–machine interface modeling. *ACS Appl. Mater. Interfaces* **13**, 3303–3310 (2021).
6. Scheibert, J., Leurent, S., Prevost, A. & Debrégeas, G. The role of fingerprints in the coding of tactile information probed with a biomimetic sensor. *Science* **323**, 1503–1506 (2009).
7. Li, X. et al. Nanotexture shape and surface energy impact on electroadhesive human–Machine interface performance. *Adv. Mater.* **33**, 2008337 (2021).
8. Zhu, M. et al. Haptic-feedback smart glove as a creative human-machine interface (HMI) for virtual/augmented reality applications. *Sci. Adv.* **6**, eaaz8693 (2020).
9. Yum, S.-M. et al. Fingerprint ridges allow primates to regulate grip. *Proc. Natl Acad. Sci.* **117**, 31665–31673 (2020).
10. Yu, X. et al. Skin-integrated wireless haptic interfaces for virtual and augmented reality. *Nature* **575**, 473–479 (2019).
11. Chortos, A., Liu, J. & Bao, Z. Pursuing prosthetic electronic skin. *Nat. Mater.* **15**, 937–950 (2016).
12. Lin, W. et al. Super-resolution wearable electrotactile rendering system. *Sci. Adv.* **8**, eabp8738 (2022).
13. Sim, K. et al. Metal oxide semiconductor nanomembrane–based soft unnoticeable multifunctional electronics for wearable human-machine interfaces. *Sci. Adv.* **5**, eaav9653 (2019).
14. Zhang, Z. et al. Active mechanical haptics with high-fidelity perceptions for immersive virtual reality. *Nat. Mach. Intell.* **5**, 643–655 (2023).
15. Yao, K. et al. Encoding of tactile information in hand via skin-integrated wireless haptic interface. *Nat. Mach. Intell.* **4**, 893–903 (2022).
16. Shultz, C. D., Peshkin, M. A. & Colgate, J. E. in *2015 IEEE world haptics conference (WHC)*. 57–62 (IEEE, 2015).
17. Shultz, C. et al. The Application of Tactile, Audible, and Ultrasonic Forces to Human Fingertips Using Broadband Electroadhesion. *IEEE Trans. Haptics* **11**, 279–290 (2018).
18. Adams, M. J. et al. Finger pad friction and its role in grip and touch. *J. R. Soc. Interface* **10**, 20120467 (2013).
19. Johnson, S., Gorman, D., Adams, M. & Briscoe, B. in *Tribology series*, Vol. 25, 663–672 (Elsevier, 1993).
20. Adams, M. J., Briscoe, B. J. & Johnson, S. A. Friction and lubrication of human skin. *Tribol. Lett.* **26**, 239–253 (2007).
21. Bowden, F. P. & Tabor, D. *The friction and lubrication of solids*. Vol. 1 (Oxford university press, 2001).
22. Persson, B., Kovalev, A. & Gorb, S. Contact mechanics and friction on dry and wet human skin. *Tribol. Lett.* **50**, 17–30 (2013).
23. Persson, B. N. General theory of electroadhesion. *J. Phys. Condens. Matter* **33**, 435001 (2021).
24. Persson, B. N. J. Contact mechanics for randomly rough surfaces. *Surf. Sci. Rep.* **61**, 201–227 (2006).
25. Ayyildiz, M., Scaraggi, M., Sirin, O., Basdogan, C. & Persson, B. N. Contact mechanics between the human finger and a touchscreen under electroadhesion. *Proc. Natl Acad. Sci.* **115**, 12668–12673 (2018).
26. Forsbach, F., Heß, M. & Papangelo, A. A two-scale FEM-BAM approach for fingerpad friction under electroadhesion. *Front. Mech. Eng.* **8**, 1074393 (2023).
27. Li, X. et al. Electrowetting: A Consideration in Electroadhesion. *IEEE Trans. Haptics* **13**, 522–529 (2020).
28. Boonpuek, P. et al. Evaluation of the electrowetting effect on the interfacial mechanics between human corneocytes and nanoasperities. *Langmuir* **37**, 4056–4063 (2021).
29. Li, X., Ma, Y., Guo, Y. & Hipwell, M. C. in *2022 IEEE Haptics Symposium (HAPTICS)*. 1–6 (IEEE, 2022).
30. Samur, E., Colgate, J. E. & Peshkin, M. A. In: *Human vision and electronic imaging XIV*. 167–173 (SPIE, 2009)
31. Peng, Y. et al. Elastohydrodynamic friction of robotic and human fingers on soft micropatterned substrates. *Nat. Mater.* **20**, 1707–1711 (2021).
32. Hamaker, H. C. The London—van der Waals attraction between spherical particles. *Physica* **4**, 1058–1072 (1937).
33. Wong, R., Geyer, S., Weninger, W., Guimberteau, J. C. & Wong, J. K. The dynamic anatomy and patterning of skin. *Exp. Dermatol.* **25**, 92–98 (2016).
34. Marks, R. & Barton, S. in *Stratum corneum*. 161–170 (Springer).
35. Berkey, C., Biniek, K. & Dauskardt, R. H. Predicting hydration and moisturizer ingredient effects on mechanical behavior of human stratum corneum. *Extrem. Mech. Lett.* **46**, 101327 (2021).
36. Yuan, Y. & Verma, R. Measuring microelastic properties of stratum corneum. *Colloids Surf. B Biointerfaces* **48**, 6–12 (2006).
37. Geerligs, M. et al. In vitro indentation to determine the mechanical properties of epidermis. *J. Biomech.* **44**, 1176–1181 (2011).
38. Gennes, P.-G., Brochard-Wyart, F. & Quéré, D. *Capillarity and wetting phenomena: drops, bubbles, pearls, waves* (Springer, 2004).
39. Lee, M., Kim, B., Kim, J. & Jhe, W. Noncontact friction via capillary shear interaction at nanoscale. *Nat. Commun.* **6**, 7359 (2015).

40. Mugele, F. & Baret, J.-C. Electrowetting: from basics to applications. *J. Phys. Condens. matter* **17**, R705 (2005).
41. Mo, Y., Turner, K. T. & Szlufarska, I. Friction laws at the nanoscale. *Nature* **457**, 1116–1119 (2009).
42. Greenwood, J. A. & Williamson, J. P. Contact of nominally flat surfaces. *Proc. R. Soc. Lond. Ser. A. Math. Phys. Sci.* **295**, 300–319 (1966).
43. Cooper, M., Mikic, B. & Yovanovich, M. M. Thermal contact conductance. *Int. J. Heat. Mass Transf.* **12**, 279–300 (1969).
44. Kogut, L. & Komvopoulos, K. Electrical contact resistance theory for conductive rough surfaces. *J. Appl. Phys.* **94**, 3153–3162 (2003).
45. Suh, A. Y. & Polycarpou, A. A. Adhesive contact modeling for sub-5-nm ultralow flying magnetic storage head-disk interfaces including roughness effects. *J Appl Phys* **97**, 104328 (2005).
46. Hasz, K., Ye, Z., Martini, A. & Carpick, R. W. Experiments and simulations of the humidity dependence of friction between nanoasperities and graphite: The role of interfacial contact quality. *Phys. Rev. Mater.* **2**, 126001 (2018).
47. Tomlinson, S., Lewis, R., Liu, X., Texier, C. & Carré, M. Understanding the friction mechanisms between the human finger and flat contacting surfaces in moist conditions. *Tribol. Lett.* **41**, 283–294 (2011).
48. Qiao, S., Li, Q. & Feng, X.-Q. Sliding friction and contact angle hysteresis of droplets on microhole-structured surfaces. *Eur. Phys. J. E* **41**, 1–8 (2018).
49. Forsberg, P. S., Priest, C., Brinkmann, M., Sedev, R. & Ralston, J. Contact line pinning on microstructured surfaces for liquids in the Wenzel state. *Langmuir* **26**, 860–865 (2010).
50. Ginn, M., Noyes, C. & Jungermann, E. The contact angle of water on viable human skin. *J. Colloid Interface Sci.* **26**, 146–151 (1968).
51. Mavon, A. et al. Sebum and stratum corneum lipids increase human skin surface free energy as determined from contact angle measurements: a study on two anatomical sites. *Colloids Surf. B Biointerfaces* **8**, 147–155 (1997).
52. Johnson, S., Adams, M., Arvanitaki, A. & Briscoe, B. in *Tribology Series* Vol. 32 199–207 (Elsevier, 1997).
53. Butler, M. D. & Vella, D. Liquid bridge splitting enhances normal capillary adhesion and resistance to shear on rough surfaces. *J. Colloid Interface Sci.* **607**, 514–529 (2022).
54. De Souza, E., Brinkmann, M., Mohrdieck, C. & Arzt, E. Enhancement of capillary forces by multiple liquid bridges. *Langmuir* **24**, 8813–8820 (2008).
55. Shultz, C. D., Peshkin, M. A. & Colgate, J. E. in *2018 IEEE Haptics Symposium (HAPTICS)*. 151–157 (IEEE, 2018).

Acknowledgements

The authors thank Dr. Yinzhong Guo with the Dow Chemical Company for providing microparticles coated plastic samples. The authors are also grateful to Dr. Mondher Cherif of Tanvas for providing the three electroadhesive touchscreens. Use of LYRA-3 Model GMH FIB-SEM, TESCAN at the TAMU Materials Characterization Facility and Dr. Sisi Xiang's assistance in the imaging with SEM are acknowledged. This work was supported by the Texas A&M Office of the President X-Grant Program: Mastering Friction to Reduce Current and Future Energy Demands, Texas A&M University; Texas A&M Engineering Experiment Station startup funds; The Governor's University Research Initiative. The Chancellor's University Research Initiative; and utilized the Texas A&M High Performance Computing Facility.

Author contributions

Y.M. and X.L. contributed equally to this work. M.C.H. and Y.M. formulated the concept; Y.M. and X.L. developed the model with supervision from M.C.H.; Y.M., X.M., and X.L. fabricated the samples with supervision from M.C.H. and S.L.; X.L., Y.M., and L. K. carried out the friction force measurements; X.L. performed contact angle measurements; C.C. acquired the finger pad topography; X.L. analyzed the data, created the figures, and prepared the original draft of the manuscript; M.C.H., Y.M., X.M., and X.L. reviewed and edited the manuscript.

Competing interests

The authors declare no competing interests.

Additional information

Supplementary information The online version contains supplementary material available at https://doi.org/10.1038/s43246-024-00724-9.

Correspondence and requests for materials should be addressed to M. Cynthia Hipwell.

Peer review information *Communications materials* thanks Lilian Hsiao and Zhuang Zhang for their contribution to the peer review of this work. Primary Handling Editor: John Plummer. A peer review file is available.

Reprints and permissions information is available at http://www.nature.com/reprints

Publisher's note Springer Nature remains neutral with regard to jurisdictional claims in published maps and institutional affiliations.

Open Access This article is licensed under a Creative Commons Attribution-NonCommercial-NoDerivatives 4.0 International License, which permits any non-commercial use, sharing, distribution and reproduction in any medium or format, as long as you give appropriate credit to the original author(s) and the source, provide a link to the Creative Commons licence, and indicate if you modified the licensed material. You do not have permission under this licence to share adapted material derived from this article or parts of it. The images or other third party material in this article are included in the article's Creative Commons licence, unless indicated otherwise in a credit line to the material. If material is not included in the article's Creative Commons licence and your intended use is not permitted by statutory regulation or exceeds the permitted use, you will need to obtain permission directly from the copyright holder. To view a copy of this licence, visit http://creativecommons.org/licenses/by-nc-nd/4.0/.

© The Author(s) 2025